Calculation of vibrational eigenenergies on a quantum computer: Application to the Fermi resonance in CO_2

Erik Lötstedt* and Kaoru Yamanouchi†
Department of Chemistry, School of Science, The University of Tokyo, 7-3-1 Hongo, Bunkyo-ku, Tokyo 113-0033, Japan

Takashi Tsuchiya and Yutaka Tachikawa
DIC Corporation, Central Research Laboratories 631, Sakado, Sakura, Chiba 285-8668, Japan

(Received 22 March 2021; accepted 4 June 2021; published 16 June 2021)

We apply a modified version of the multistate contracted variational quantum eigensolver method to calculate vibrational eigenstates of CO_2 on a quantum computer. A two-mode model of CO_2 is employed, and the vibrational wave function is expanded using three harmonic-oscillator basis functions for each mode. The wave functions are mapped to four qubits by a compact mapping method. The Hamiltonian matrix elements are evaluated on a simulator including noise and on a quantum computer available at IBM Quantum, while the Hamiltonian matrix is diagonalized on a classical computer. We propose an error mitigation method by which the shift of the numerical values of the matrix elements originating from the noise can be corrected, and examine the dependence of the statistical uncertainties on the number of executions of each quantum circuit. We find that, at about 8×10^6 executions, the energy eigenvalues of the Fermi resonance states in CO_2 can be obtained with an uncertainty within 1 cm^{-1}.

DOI: 10.1103/PhysRevA.103.062609

I. INTRODUCTION

The calculation of energy levels of quantum-mechanical systems is one of the promising applications of future quantum computers [1,2]. At present, even though a quantum computational advantage has been demonstrated using 53 superconducting qubits [3] and a 100-mode photonic interferometer [4], quantum chemistry calculations have been carried out for only relatively small quantum systems containing a few particles using quantum computers having up to 10 qubits. Recently, a Hartree-Fock calculation of the potential-energy curve of a linear chain of 12 hydrogen atoms (H_{12}) was demonstrated using 12 qubits [5]. It is highly awaited that much larger and much less noisy quantum computers will be available in the future, which motivates the development of algorithms and methods using quantum computers presently available for their implementations in the future.

Thus far, the main focus of research in quantum chemistry using quantum computers has been the electronic eigenvalue problem, where the positions of the nuclei in the molecule are treated as parameters. Potential-energy curves of H_2 [6–10], HeH^+ [11], LiH [8,10], and BeH_2 [8] have been obtained using quantum computers.

On the other hand, the vibrational eigenvalue problem has received much less attention. Even if we can obtain the potential-energy surface of a molecule, a complete discussion of the dynamics of the molecule must include the vibrational motion, which should be treated quantum mechanically. Because a nonlinear molecule having N atoms has $3N-6$ vibrational degrees of freedom, if we assign a basis set of size κ to each degree of freedom, we have to diagonalize a $\kappa^{3N-6} \times \kappa^{3N-6}$ matrix to obtain the vibrational eigenenergies. Because of the exponential increase of the matrix size with N, obtaining all the bound vibrational levels on a classical computer is possible only for molecules having up to $N = 5$ atoms [12,13]. In the case of a quantum computer, where K qubits can store an exponentially large number (2^K) of amplitudes, the vibrational wave functions can be represented even for large molecules having a large N, suggesting that the vibrational eigenenergies can be obtained for gigantic molecular systems that cannot be treated by classical computers.

A general discussion of how to map the quantum-mechanical vibrational Hamiltonian to qubits has been reported in Refs. [14,15], with application to triatomic molecules (H_2O [14] and H_2O, SO_2, and NO_2 [15]). In Ref. [16], an approach based on modal basis functions was introduced, and a few vibrationally excited states of CO_2 were computed. We also note that a method referred to as bosonic sampling may enable efficient evaluation of the Franck-Condon factors in vibronic transitions [17–19].

In the present study, in order to explore future applications of quantum computers to molecular vibrational spectroscopy, we apply a modified version of the multistate contracted variational quantum eigensolver (MC-VQE) method to the calculation of a few low-lying vibrational eigenstates of carbon dioxide (CO_2), one of the typical linear triatomic molecular species. The MC-VQE method was proposed in Ref. [20] as a method for calculating electronic transition energies. We find that a suitably adapted version of the MC-VQE method gives good results also when it is applied to the

*lotstedt@chem.s.u-tokyo.ac.jp
†kaoru@chem.s.u-tokyo.ac.jp

calculation of vibrational eigenenergies. Differently from available eigenvalue methods such as the phase estimation method [21,22] and the Trotterized adiabatic quantum computing approach [23–25], in both of which multiple operations of the time evolution operator are involved so that quantum circuits would become very long, the circuits required in the MC-VQE method are much shorter and suitable for the execution on presently available quantum computers.

We implement the MC-VQE method using a compact mapping of the vibrational Hamiltonian to a qubit form. The performance of the method is assessed for the ideal noise-free case, for a simulator including the noise model *FakeRome* as implemented in QISKIT [26], and for the *ibmq_rome* quantum computer at IBM Quantum [27].

The vibrational mode coupling in CO_2 is characterized by a well-known strong 1:2 anharmonic resonance, called a Fermi resonance [28,29]. The Fermi resonance in CO_2 refers to the strong mixing of the wave function where the symmetric stretching ν_1 mode is singly excited and the wave function where the bending ν_2 mode is doubly excited, and appears in the Raman spectrum as a double peak at 1285 cm^{-1} and 1388 cm^{-1}. The 1:2 Fermi resonance is a good test case for an eigenvalue method implemented on a quantum computer because it is an example of the most fundamental anharmonic resonances, which exist universally in the vibrationally excited states of polyatomic molecules and play a decisive role in intramolecular vibrational energy redistribution (IVR) processes [30] and unimolecular reactions [31].

II. THEORY

A. Vibrational Hamiltonian and qubit mapping

We consider a two-mode model of CO_2, represented by the vibrational Hamiltonian

$$H = H_0 + H_I = \sum_{i=1}^{2} \frac{\omega_i}{2}\left(-\frac{\partial^2}{\partial q_i^2} + q_i^2 - 1\right) + \sum_{i\leqslant j\leqslant l} k_{ijl} q_i q_j q_l, \qquad (1)$$

where q_i is a dimensionless normal mode coordinate, ω_i is the harmonic frequency of mode i, and k_{ijl} are anharmonic coupling coefficients. The ν_1 mode is the symmetric stretching mode and ν_2 is the bending mode. Note that we have subtracted the zero-point energy so that the ground-state energy is zero in absence of the anharmonic coupling. The numerical values for the harmonic frequencies ω_i and the anharmonic coupling coefficients k_{ijl} in Eq. (1) are taken to be the experimentally determined values reported in Ref. [32], and are given as $\omega_1 = 1354.31$ cm^{-1}, $\omega_2 = 672.85$ cm^{-1}, $k_{111} = -45.78$ cm^{-1}, $k_{122} = 74.72$ cm^{-1}, and $k_{112} = k_{222} = 0$. The coefficients k_{112} and k_{222} vanish because the molecular potential is an even function of the bending coordinate q_2. We express energy in units of cm^{-1}, as is conventionally done in vibrational spectroscopy. For the conversion to other commonly employed energy units, we have 1 eV $\approx$ 8065.54 cm^{-1} and 1 a.u. $\approx$ 219475 cm^{-1}.

We employ harmonic-oscillator eigenfunctions $|v_2, v_1\rangle$ satisfying

$$H_0|v_2, v_1\rangle = (\omega_2 v_2 + \omega_1 v_1)|v_2, v_1\rangle \qquad (2)$$

as basis functions, and consider $0 \leqslant v_1, v_2 \leqslant v_{\max} = 2$. The nth eigenstate $|\psi_n\rangle$ of the Hamiltonian H is expanded as

$$|\psi_n\rangle = \sum_{v_2,v_1=0}^{v_{\max}} c^n_{v_2 v_1} |v_2, v_1\rangle. \qquad (3)$$

The Fermi resonance occurs because of the nonzero value of k_{122} and the approximate equality $\omega_1 \approx 2\omega_2$, resulting in a strong mixing of the $|2, 0\rangle$ and $|0, 1\rangle$ levels.

We consider the compact mapping [14,33], which is also called binary mapping, as the method of mapping the wave function and Hamiltonian to a qubit form. For our two-mode model with $v_{\max} = 2$, we need four qubits to represent the vibrational wave function. A brief discussion on the mapping method and explicit expressions for the qubit Hamiltonian can be found in Appendix A.

B. MC-VQE method

The MC-VQE method, which we are now going to use for the calculation of vibrational energy levels, was proposed in [20] as a method for obtaining electronic transition energies of molecules, and is a method which can be used to obtain a few low-lying eigenstates out of a large Hilbert space.

The MC-VQE method is based on an extension of the variational quantum eigensolver (VQE) idea [34–37]. First, we define a set of basis functions represented as circuits on the quantum computer. The basis set is parametrized by a parameter $\boldsymbol{\theta}$, which is chosen so that the sum of the ground- and excited-state energies is minimized. Second, we construct a Hamiltonian matrix by evaluating the matrix elements on the quantum computer. Third, we obtain estimates of the energy eigenvalues by diagonalizing the Hamiltonian matrix on a classical computer.

We define a set of $\boldsymbol{\theta}$-dependent basis functions as

$$|\chi_n\rangle = U(\boldsymbol{\theta})|\phi_n\rangle, \quad n = 0, \ldots, 2v_{\max} = 4, \qquad (4)$$

where $U(\boldsymbol{\theta})$ is a unitary operator depending on a set of parameters $\boldsymbol{\theta} = (\theta_1, \theta_2, \ldots)$ and $\{|\phi_n\rangle\}$ is a set of single-mode excited states,

$$|\phi_n\rangle = \begin{cases} |0, 0\rangle & \text{if } n = 0, \\ |0, n\rangle & \text{if } 0 < n \leqslant v_{\max}, \\ |n - v_{\max}, 0\rangle & \text{if } v_{\max} < n \leqslant 2v_{\max}. \end{cases} \qquad (5)$$

The role of the unitary operator $U(\boldsymbol{\theta})$ is to introduce contributions from double-mode excitations in the basis set without increasing the number of basis functions, so that the descriptions of both the ground and the excited states are improved. Note that, for a polyatomic molecule having many modes, $U(\boldsymbol{\theta})$ introduces contributions not only from the double-mode excitation but also multimode excitations such as triple-mode and quadruple-mode excitations. The parametrization of $U(\boldsymbol{\theta})$ is chosen such that $U(\boldsymbol{\theta} = \mathbf{0})$ equals the identity operator.

After having defined the basis set, we construct the Hamiltonian matrix $\boldsymbol{h}$ with matrix elements

$$h_{mn} = \langle\chi_m|H|\chi_n\rangle = \langle\phi_m|U^\dagger(\boldsymbol{\theta})HU(\boldsymbol{\theta})|\phi_n\rangle \qquad (6)$$

by evaluating h_{mn} on the quantum computer. The technique for evaluating h_{mn} is described in Appendix B. We obtain the vibrational eigenvalues E_n by diagonalizing the matrix $\boldsymbol{h}$ on a

classical computer,

$$\boldsymbol{h} = \boldsymbol{b}\boldsymbol{E}\boldsymbol{b}^{\dagger}, \tag{7}$$

where the columns of $\boldsymbol{b}$ contain the eigenvectors and $\boldsymbol{E}$ is a diagonal matrix with the eigenenergies on the diagonal. In the present example of a two-mode model of CO_2 using $v_{\max} + 1 = 3$ basis functions per mode, we need to diagonalize a $(2v_{\max} + 1) \times (2v_{\max} + 1) = 5 \times 5$ matrix.

The optimal value of $\boldsymbol{\theta}$ is determined so that the sum S of the eigenenergies,

$$S = \sum_{n=0}^{2v_{\max}} E_n, \tag{8}$$

is minimized. By Eq. (7), we see that S can be written as

$$S = \mathrm{Tr}\boldsymbol{h} = \sum_{n=0}^{2v_{\max}} h_{nn}, \tag{9}$$

which means that, in the optimization procedure, we only need to evaluate the diagonal elements of $\boldsymbol{h}$. The strength of the MC-VQE method is that all energy levels are considered in the energy optimization, so that both the ground-state and excited-state wave functions are treated on an equal footing. In addition, the same set of basis functions is used for both ground and excited states, which guarantees mutual orthogonality among the ground- and excited-state wave functions.

In the original publication [20], the unitary operator $U(\boldsymbol{\theta})$ was expressed as a combination of general SO(4) operators acting pairwise on two qubits, which was suitable for the exciton model considered in Ref. [20]. For vibrational eigenvalue calculations, we use the exponentiated unitary coupled-cluster operator as $U(\boldsymbol{\theta})$,

$$U(\boldsymbol{\theta}) = e^{T(\boldsymbol{\theta}) - T^{\dagger}(\boldsymbol{\theta})}, \tag{10}$$

where T is the cluster operator. The unitary coupled-cluster (UCC) ansatz [38,39] is a widely used ansatz in VQE approaches for the calculation of electronic eigenenergies [7,34,40–42], and has also been proposed for the evaluation of the vibrational eigenvalues [16]. In the present investigation, we include single excitation operators in the cluster operator T and write

$$T(\boldsymbol{\theta}) - T^{\dagger}(\boldsymbol{\theta}) = \sum_{\ell=1}^{2} \sum_{v',v=0}^{v_{\max}} \theta^{\ell}_{v'v} |v'\rangle\langle v|_{\ell}, \tag{11}$$

where $|v'\rangle\langle v|_{\ell}$ is a single excitation operator for mode ℓ. We have for example $|v'\rangle\langle v|_1|v_2, v_1\rangle = \delta_{v_1 v}|v_2, v'\rangle$. The parameter matrix $\theta^{\ell}_{v'v}$ is a real-valued antisymmetric matrix satisfying $\theta^{\ell}_{v'v} = -\theta^{\ell}_{vv'}$.

We find that, for the Hamiltonian (6), it is sufficient to consider the parameter $\theta^1_{01} \equiv \theta$ as a variational parameter, and set the remaining part of $\theta^{\ell}_{v'v}$ to be zero. We have confirmed that the eigenenergies are lowered by only less than 0.2 cm^{-1} if all parameters $\theta^{\ell}_{v'v}$ are allowed to be varied in Eq. (11). We therefore employ the following form of $U(\boldsymbol{\theta})$,

$$U(\theta) = e^{\theta(|0\rangle\langle 1|_1 - |1\rangle\langle 0|_1)}, \tag{12}$$

in the discussion below in Sec. III.

The advantage of the MC-VQE method executed on a quantum computer originates from choosing the unitary operator $U(\boldsymbol{\theta})$ such that the matrix elements h_{mn} are difficult to evaluate on a classical computer, but can be efficiently evaluated on a quantum computer. This is true in our case with $U(\boldsymbol{\theta})$ being the unitary coupled-cluster operator, which cannot be implemented efficiently on a classical computer when the number of vibrational modes $V = 3N - 6$ is large. In order to implement $U(\boldsymbol{\theta})$ on a classical computer, we have to represent $U(\boldsymbol{\theta})$ as a full CI matrix of exponentially large size $\kappa^V \times \kappa^V$ [43], where κ is the number of basis functions for each mode. On a quantum computer, we estimate (see Appendix C for a detailed discussion) that the total number of circuits N_{circ} and the total number of controlled-NOT (CNOT) gates N_{CNOT} in each circuit scale polynomially in V as

$$N_{\mathrm{circ}} = O(V^{p+2}\kappa^{2p+2}) \tag{13}$$

and

$$N_{\mathrm{CNOT}} = O(V^{c}\kappa^{3c}\log_2\kappa), \tag{14}$$

where p is the highest order of the anharmonic coupling term in the Hamiltonian and c is the excitation order of the unitary coupled-cluster operator. In the case considered in the present paper, we have $p = 3$ and $c = 1$.

III. RESULTS

We implement the four-qubit quantum circuits necessary for the evaluation of the matrix $\boldsymbol{h}$ using QISKIT [26]. For most of the results shown in this section, we evaluate the circuits using the simulator *qasm_simulator* and the error model *FakeRome*. The error model includes incoherent single-gate errors in the form of a depolarizing channel combined with a single-qubit thermal relaxation channel and readout errors [26,44,45]. We also present data obtained with the *ibmq_rome* five-qubit quantum computer at IBM Quantum [27]. The depth of the longest circuit is 10 and the maximum number of CNOT gates is three. Unless otherwise indicated, each circuit is executed $N_{\mathrm{shots}} = 8192$ times (the largest value possible at IBM Quantum). Because of the finite value of N_{shots}, the matrix elements carry an intrinsic statistical uncertainty, which is present even in the absence of the incoherent single-gate errors and the readout errors. One matrix element h_{mn} requires the execution of 25 circuits when $m = n$ and 49 circuits when $m \neq n$.

In order to estimate the statistical uncertainty due to the finite value of N_{shots}, we repeat the evaluation of $\boldsymbol{h}$ 1000 times ($M = 1000$), and record a histogram of each matrix element. The statistical uncertainty of the matrix elements is estimated as the square root of the variance of the data. The average value of the matrix $\boldsymbol{h}$ after the evaluations for M times is denoted by $\overline{\boldsymbol{h}}$, whose matrix elements are $\overline{h}_{mn}$.

A. Error mitigation

We employ the following four methods to reduce the error in the evaluation of $\boldsymbol{h}$.

(i) Only matrix elements h_{mn} with $m \leqslant n$ are evaluated. The remaining part of the matrix is filled by using $h_{mn} = h_{nm}$, so that $\boldsymbol{h}$ is guaranteed to be a symmetric matrix.

(ii) Matrix elements vanishing identically are not evaluated, but set to be zero. If we write the Hamiltonian matrix as

$$h_{mn} = h^0_{mn} + h^I_{mn} = \langle \chi_m | H_0 | \chi_n \rangle + \langle \chi_m | H_I | \chi_n \rangle, \tag{15}$$

the only nonvanishing matrix elements of h^0_{mn} are $h^0_{01} = h^0_{10} \neq 0$ and the diagonal matrix elements $h^0_{mm} \neq 0$. For h^I_{mn}, the matrix elements vanishing identically are $h^I_{03} = h^I_{13} = h^I_{23} = h^I_{34} = 0$. For example, we have

$$U(\theta)|v_2, 0\rangle = \cos\theta |v_2, 0\rangle - \sin\theta |v_2, 1\rangle. \tag{16}$$

It follows that

$$h_{03} = \langle 0, 0 | U^\dagger(\theta) H U(\theta) | 1, 0 \rangle = 0, \tag{17}$$

because the Hamiltonian (1) contains only even orders of q_2 and cannot couple basis functions $|v_2, v_1\rangle$, $|v_2', v_1'\rangle$, where v_2 is even and v_2' is odd.

(iii) In the evaluation of the matrix elements h^0_{mn} of the harmonic-oscillator part H_0 of the Hamiltonian (1), we discard measurements of a circuit resulting in a qubit state which does not represent a basis function. For example, the evaluation of the matrix elements of H_0 involves expectation values like

$$z = \langle \psi | \sigma_z(0) | \psi \rangle, \tag{18}$$

where $|\psi\rangle$ is a wave function represented by a quantum circuit and $\sigma_z(0)$ is a Pauli operator acting on qubit 0. Without error mitigation, we would estimate z by measuring the circuit representing $|\psi\rangle$ N_{shots} times and calculating

$$z = \frac{n_0 - n_1}{N_{\text{shots}}}, \tag{19}$$

where n_i is the number of measurements where qubit 0 was measured as i. In our error mitigation scheme, we measure all the qubits and discard the measurements where the measured qubit state is outside the Hilbert space spanned by the basis functions adopted in the model. This means that we discard measurements where either qubits 0 and 1 are measured as $q_1q_0 = 11$ or qubits 2 and 3 are measured as $q_3q_2 = 11$. For example, we discard the measurements when the set of four qubits are $q_3q_2q_1q_0 = 0011$ because this qubit state $|00\ 11\rangle$ corresponds to the vibrational basis function $|v_2 = 0, v_1 = 3\rangle$ whose vibrational quantum number, v_1, exceeds the upper limit of $v_{\max} = 2$. The expectation value (18) is evaluated as

$$z = \frac{\tilde{n}_0 - \tilde{n}_1}{N_{\text{shots}} - N_{\text{e}}}, \tag{20}$$

where $\tilde{n}_i$ is the number of measurements where qubit 0 was measured as i after discarding the erroneous measurements and N_{e} is the total number of the erroneous measurements.

(iv) Error corrections are made by comparison with the Hamiltonian matrix evaluated at $\theta = 0$. Errors in the execution of the quantum circuits result in a shift of the matrix elements from the exact values. As will be demonstrated below in Sec. III B, the shift can be assumed to be independent of θ to a good approximation. Thus we have

$$\boldsymbol{h}(\theta) \approx \boldsymbol{h}_{\text{exact}}(\theta) + \boldsymbol{\Delta}, \tag{21}$$

where $\boldsymbol{h}(\theta)$ is the matrix evaluated on the quantum computer, $\boldsymbol{h}_{\text{exact}}(\theta)$ is the numerically exact value of the Hamiltonian matrix (6), and $\boldsymbol{\Delta}$ is a constant matrix. Assuming that the shift $\boldsymbol{\Delta}$ is θ independent, we can estimate $\boldsymbol{\Delta}$ at $\theta = 0$,

$$\boldsymbol{\Delta} = \boldsymbol{h}_{\text{exact}}(0) - \boldsymbol{h}(0). \tag{22}$$

The idea is that, although we cannot evaluate $\boldsymbol{h}_{\text{exact}}(\theta)$ classically in the general case of a polyatomic molecule having a large number of vibrational degrees of freedom, $\boldsymbol{h}_{\text{exact}}(\theta = 0)$ can be evaluated on a classical computer because it involves the matrix elements between single-mode excited basis states. For a nonlinear molecule having N atoms having $3N - 6$ vibrational degrees of freedom, there are a total of $\kappa_{\text{s}} = (3N - 6)(\kappa - 1) + 1$ single-mode excited states if we assume that κ basis functions are used to describe each mode. Because κ_{s} scales linearly with N, it is feasible to adopt this error mitigation method via the calculation of $\boldsymbol{h}_{\text{exact}}(\theta = 0)$ even for larger-sized polyatomic molecules with $N \gg 1$.

Based on the above considerations, we propose the following error mitigation scheme, labeled as scheme (iv). First, we evaluate $\boldsymbol{h}_{\text{exact}}(\theta = 0)$ classically and $\bar{\boldsymbol{h}}(\theta = \theta_0)$ on the quantum computer, where θ_0 is a small number of the order of 10^{-5}. We cannot use $\theta_0 = 0$ because, as explained in the next Sec. III B, the constant shift $\boldsymbol{\Delta}$ obtained when θ is exactly equal to zero is different from that obtained when θ is very close to zero but not exactly zero. Second, the constant shift $\boldsymbol{\Delta}_0$ is evaluated according to

$$\boldsymbol{\Delta}_0 = \boldsymbol{h}_{\text{exact}}(0) - \bar{\boldsymbol{h}}(\theta_0) \tag{23}$$

and the corrected Hamiltonian matrix $\boldsymbol{h}'(\theta)$ is calculated as

$$\boldsymbol{h}'(\theta) = \boldsymbol{h}(\theta) - \boldsymbol{\Delta}_0. \tag{24}$$

We remark that the error mitigation method described above can be applied when θ is sufficiently small, so that the shift $\boldsymbol{\Delta}_0$ is approximately the same for all θ.

A commonly employed error mitigation approach, which is an alternative to the scheme (iv) described above, is to introduce controlled amounts of additional noise into the quantum circuit, measure the circuit at various values of the noise, and finally extrapolate to zero noise [46–49]. We have used the error mitigation method (iv) in the present investigation because of the simplicity of its implementation.

B. Optimal value of θ

In Fig. 1, we show the sum of the eigenenergies, $S = \text{Tr}\bar{\boldsymbol{h}}$, as a function of θ, obtained using the *qasm_simulator* and the error model *FakeRome*. The S value is evaluated at $\theta = 0$, 10^{-5}, 0.005, 0.01, ..., 0.10. The value $\theta = 10^{-5}$ is added to illustrate the difference between $\theta = 0$ and a small but nonzero value of θ. The S value evaluated using a combination of the three error mitigation methods (i), (ii), and (iii) is shown in Fig. 1(a). We observe that S evaluated by the simulator is larger than the exact value of S by about 210 cm^{-1}. We also see that the shift of $S(\theta = 0)$ is different from the shift of $S(\theta > 0)$. This is because, at $\theta = 0$, the unitary operator $U(\theta = 0) = 1$ and the quantum circuit used for the evaluation of $\boldsymbol{h}$ is simplified. In Fig. 1(b), we show the summed energy evaluated using a combination of the four error mitigation methods (i), (ii), (iii), and (iv). After the error correction, the curve obtained using the simulator agrees well with the exact curve.

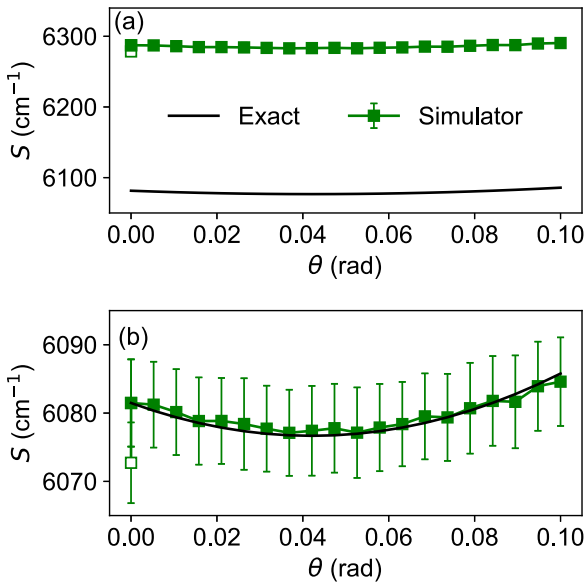

FIG. 1. Sum of the excited-state energies S as a function of the variational parameter θ. The value of $S(\theta = 0)$ is shown with open squares and the values of $S(\theta > 0)$ are shown with filled squares. (a) Without subtraction of the constant shift $\mathbf{\Delta}_0$; (b) after error mitigation by subtraction of a constant energy shift $\mathbf{\Delta}_0$ [see Eq. (24)]. The curve labeled "Exact" refers to the numerically exact value of S calculated with a classical computer. The lengths of the error bars correspond to the square root of the variance. The legend in panel (a) applies also to panel (b).

In order to demonstrate that the matrix elements $\overline{h}_{mn}$ are approximately constant as a function of θ, as required in the error mitigation scheme described in Sec. III A, we show the matrix elements $\Delta_{mn}(\theta)$ of the difference matrix $\mathbf{\Delta}$ in Fig. 2, where $\mathbf{\Delta}(\theta)$ is defined as

$$\mathbf{\Delta}(\theta) = \overline{\boldsymbol{h}}(\theta) - \boldsymbol{h}_{\text{exact}}(\theta). \tag{25}$$

The curves of $\Delta_{mn}(\theta)$ in Fig. 2 clearly show that $\mathbf{\Delta}(\theta)$ is approximately constant over the range $10^{-5} \leqslant \theta \leqslant 0.10$.

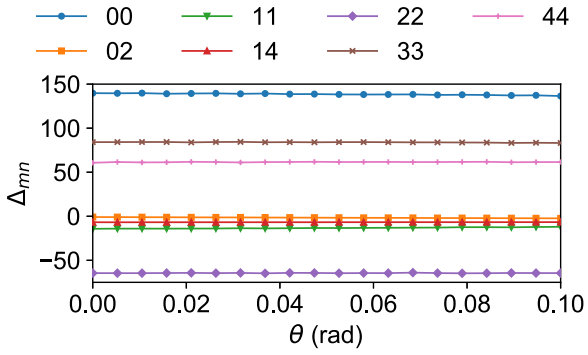

FIG. 2. Difference Δ_{mn} of the Hamiltonian matrix evaluated on the quantum computer and the exact Hamiltonian [see definition in Eq. (25)] as a function of the variational parameter θ. The legend indicates the indices mn. Δ_{mn} is shown only when the matrix element $h_{mn} > 1$ cm^{-1}. The statistical uncertainties as measured by the square root of the variances are smaller than 8 cm^{-1} for all curves, and are not shown in the figure.

We have confirmed that the change of $\Delta_{mn}(\theta)$ is less than 4 cm^{-1} over the range $10^{-5} \leqslant \theta \leqslant 0.10$ for all matrix elements shown in Fig. 2. This means that the average Hamiltonian matrix $\overline{\boldsymbol{h}}$ is shifted from the exact Hamiltonian $\boldsymbol{h}_{\text{exact}}$ by an amount of energy which is approximately independent of θ.

We can see in Fig. 1(b) that the optimal value of θ is close to 0.04. For the results shown in the remainder of this paper, we have therefore used $\theta = 0.04$ in the evaluation of $\boldsymbol{h}$. In the present investigation, the wave-function ansatz depends on one parameter only, so that the optimal value of θ can be inferred from the minimum of a one-dimensional curve. In the general case in which the wave-function ansatz depends on several parameters, we have to consider a suitable optimization algorithm and examine the effect of noise on the minimization procedure as has been discussed before [34,50–52].

C. Eigenenergy evaluation

As described in Sec. III A, we obtain the corrected Hamiltonian matrix $\boldsymbol{h}'$ (evaluated at $\theta = 0.04$) by subtracting a constant shift from the uncorrected Hamiltonian matrix $\boldsymbol{h}$ [see Eq. (24)]. The evaluation of $\boldsymbol{h}'$ is repeated $M = 1000$ times, so that we obtain M sample Hamiltonians $\boldsymbol{h}'(1), \ldots, \boldsymbol{h}'(M)$. The average Hamiltonian $\overline{\boldsymbol{h}}'$ is defined as

$$\overline{\boldsymbol{h}}' = \frac{1}{M}\sum_{i=1}^{M} \boldsymbol{h}'(i) \tag{26}$$

and the statistical uncertainty of each matrix element is defined as

$$\tau_{mn} = \sqrt{\frac{1}{M-1}\sum_{i=1}^{M}[h'_{mn}(i) - \overline{h}'_{mn}]^2}. \tag{27}$$

The final estimate $\overline{E}_n$ ($n = 0, \ldots, 2v_{\max} = 4$) of the energy eigenvalues evaluated by the quantum computer is given by the diagonalization of $\overline{\boldsymbol{h}}'$ as

$$\overline{E}_n = \boldsymbol{b}_n^{\dagger}\overline{\boldsymbol{h}}'\boldsymbol{b}_n, \tag{28}$$

where $\boldsymbol{b}_n$ is the nth eigenvector of $\overline{\boldsymbol{h}}'$.

The statistical uncertainty of the eigenvalues calculated from an ensemble of random matrices $\boldsymbol{h}'(i)$ can be estimated as follows. We first write

$$\boldsymbol{h}' = \overline{\boldsymbol{h}}' + \boldsymbol{\delta}, \tag{29}$$

where $\boldsymbol{\delta}$ is a random symmetric matrix with matrix elements denoted by δ_{mn} and where each matrix element has an average value $\overline{\delta}_{mn} = 0$ and the width τ_{mn} given by Eq. (27). If we assume that each matrix element τ_{mn} is small, we obtain by first-order perturbation theory

$$\begin{aligned} E_n &\approx \overline{E}_n + \boldsymbol{b}_n{}^{\dagger}\boldsymbol{\delta}\boldsymbol{b}_n \\ &= \overline{E}_n + \sum_{m=0}^{4} b_{mn}^2\delta_{mm} + 2\sum_{\substack{l=0 \\ m>l}}^{4} b_{ln}b_{mn}\delta_{lm}, \end{aligned} \tag{30}$$

where in the last equality we have used the symmetry $\delta_{mn} = \delta_{nm}$. It follows from Eq. (30) that the statistical uncertainty of

TABLE I. Energy eigenvalues in units of cm^{-1}. The numbers in parentheses in the "Simulator" row are the statistical uncertainties estimated by Eq. (32).

	E_0	E_1	E_2	E_3
Simulator	−0.68(19)	672.19(19)	1307.35(13)	1381.81(11)
Exact ($\theta = 0.04$)	−0.36	672.56	1307.03	1381.47
Exact ($\theta = 0$)	−0.36	672.85	1309.25	1383.78
Full CI	−0.88	672.15	1306.27	1380.56

E_n denoted as w_n can be estimated as

$$w_n = \sqrt{\sum_{m=0}^{4} b_{mn}^4 \tau_{mm}^2 + 4 \sum_{\substack{l=0 \\ m>l}}^{4} b_{ln}^2 b_{mn}^2 \tau_{lm}^2}. \tag{31}$$

For the statistical uncertainty $\overline{\sigma}_n$ of the eigenenergies $\overline{E}_n$ that we obtain by diagonalizing the average Hamiltonian $\overline{\boldsymbol{h}}'$, we have

$$\overline{\sigma}_n = \frac{w_n}{\sqrt{M}}. \tag{32}$$

In order to visualize the distribution of eigenvalues, we also obtain energy eigenvalues $E_n^{(i)}$ ($n = 0, \ldots, 2v_{\max} = 4$ and $i = 1, \ldots, M$) by diagonalizing each $\boldsymbol{h}'(i)$. The average $\widetilde{E}_n$ over the M values of $E_n^{(i)}$ is defined as

$$\widetilde{E}_n = \frac{1}{M} \sum_{i=1}^{M} E_n^{(i)}. \tag{33}$$

The statistical uncertainty of $E_n^{(i)}$ denoted as σ_n is defined as the square root of the variance of $E_n^{(i)}$,

$$\sigma_n = \sqrt{\frac{1}{M-1} \sum_{i=1}^{M} \left[E_n^{(i)} - \widetilde{E}_n\right]^2}. \tag{34}$$

We note that $\overline{E}_n \neq \widetilde{E}_n$ in general, because the energy eigenvalues are nonlinear functions of the matrix elements h'_{mn}. In the present investigation, however, $\overline{E}_n \approx \widetilde{E}_n$ (we have $|\overline{E}_n - \widetilde{E}_n| < 0.2$ cm^{-1} for all n) because of the small statistical uncertainty. We also find that $\sigma_n \approx w_n$ (we have $|\sigma_n - w_n| < 0.1$ cm^{-1} for all n), and, therefore, both σ_n and w_n can be used as measures of the statistical uncertainty of the resultant eigenenergies.

In Fig. 3, we show a histogram of the energy eigenvalues E_n for $n \leqslant 3$, as well as the energies $\overline{E}_n$, obtained using the *qasm_simulator* and the error model *FakeRome*. We also show the energy eigenvalues obtained by $M = 13$ evaluations of $\boldsymbol{h}'$ using the *ibmq_rome* quantum computer at IBM Quantum. The energy levels of the ground state, E_0, and that of the first excited state, E_1, have the corresponding wave functions $|\psi_0\rangle \approx |0, 0\rangle$ and $|\psi_1\rangle \approx |1, 0\rangle$, respectively. The energy levels E_2 and E_3 are the two energy levels involved in the Fermi resonance and have the approximate wave functions $|\psi_2\rangle \approx (|0, 1\rangle - |2, 0\rangle)/\sqrt{2}$ and $|\psi_3\rangle \approx (|0, 1\rangle + |2, 0\rangle)/\sqrt{2}$. The basis functions $|0, 1\rangle$ and $|2, 0\rangle$ appear with almost equal weight in $|\psi_2\rangle$ and $|\psi_3\rangle$ because the anharmonic coupling matrix element $\langle 0, 1|H_I|2, 0\rangle = 37.36$ cm^{-1} is larger than the unperturbed energy gap $\omega_1 - 2\omega_2 = 8.61$ cm^{-1}.

For comparison, we also show the following reference energy values in Fig. 3.

(i) The numerically exact energy $E_n^{\mathrm{exact}}(\theta)$ resulting from the diagonalization of the exact Hamiltonian defined in Eq. (6). We show $E_n^{\mathrm{exact}}(\theta)$ for $\theta = 0$ and $\theta = 0.04$, labeled by "Exact ($\theta = 0$)" and "Exact ($\theta = 0.04$)." $E_n^{\mathrm{exact}}(\theta = 0)$ represents the energy obtained using unmodified single-mode excited states as basis functions and can be calculated efficiently on a classical computer. $E_n^{\mathrm{exact}}(\theta = 0.04)$ represents the energy which would be obtained on a quantum computer in the absence of noise and in the limit of $N_{\mathrm{shots}} \to \infty$.

(ii) The energy E_n^{FCI}, which is the full configuration-interaction (full CI) energy obtained by including all nine basis functions $|v_2, v_1\rangle$, $0 \leqslant v_1, v_2 \leqslant 2$ in the wave-function expansion. The energy E_n^{FCI} represents the best possible energy obtainable given the basis set $|v_2, v_1\rangle$ ($0 \leqslant v_1, v_2 \leqslant 2$) and is labeled by "Full CI" in Fig. 3. Because of the limited size of the present model system, we can obtain both $E_n^{\mathrm{exact}}(\theta)$ and E_n^{FCI} exactly on a classical computer.

We can see that the eigenenergies of the average Hamiltonian obtained by the *qasm_simulator* at $\theta = 0.04$ are very close to the exact energies. We have $|E_0^{\mathrm{exact}}(0.04) - \overline{E}_0| = 0.32$ cm^{-1}, $|E_1^{\mathrm{exact}}(0.04) - \overline{E}_1| = 0.37$ cm^{-1}, $|E_2^{\mathrm{exact}}(0.04) - \overline{E}_2| = 0.32$ cm^{-1}, and $|E_3^{\mathrm{exact}}(0.04) - \overline{E}_2| = 0.34$ cm^{-1}, demonstrating that, after the error correction, an uncertainty of below 1 cm^{-1} can be obtained with the MC-VQE method combined with the compact qubit mapping. The uncertainty is defined as the difference between the eigenvalues $\overline{E}_n$ evaluated on the quantum computer and the exact eigenvalues E_n^{exact} evaluated on the classical computer. The numerical values of $\overline{E}_n$, $E_0^{\mathrm{exact}}(\theta = 0, 0.04)$, and E_n^{FCI} are summarized in Table I. In Ref. [16], the vibrational ground-state energy of CO_2 was obtained with an uncertainty of about 100 cm^{-1} using the Compact Heuristic for Chemistry (CHC) wave function ansatz and an error model with parameters from the *ibmq_almaden* device, with no error mitigation.

For the ground state and the first excited state, the effect of introducing the θ-dependent basis set defined in Eq. (4) is rather small. We have $E_0^{\mathrm{exact}}(\theta = 0) - E_0^{\mathrm{exact}}(\theta = 0.04) = 3 \times 10^{-4}$ cm^{-1} and $E_1^{\mathrm{exact}}(\theta = 0) - E_1^{\mathrm{exact}}(\theta = 0.04) = 0.3$ cm^{-1}. On the other hand, the Fermi resonance state energies are lowered by about 2 cm^{-1} by introducing a θ-dependent basis set (4) with $\theta = 0.04$. This means that, in order to discuss if the improvement is achieved when using $\theta = 0.04$ compared with $\theta = 0$, we have to reduce the uncertainty of the energies calculated using the quantum computer to be smaller than 1 cm^{-1}. Indeed, as shown in Table I, the uncertainties are all smaller than 1 cm^{-1} for all energy eigenvalues, which fulfills the present requirement.

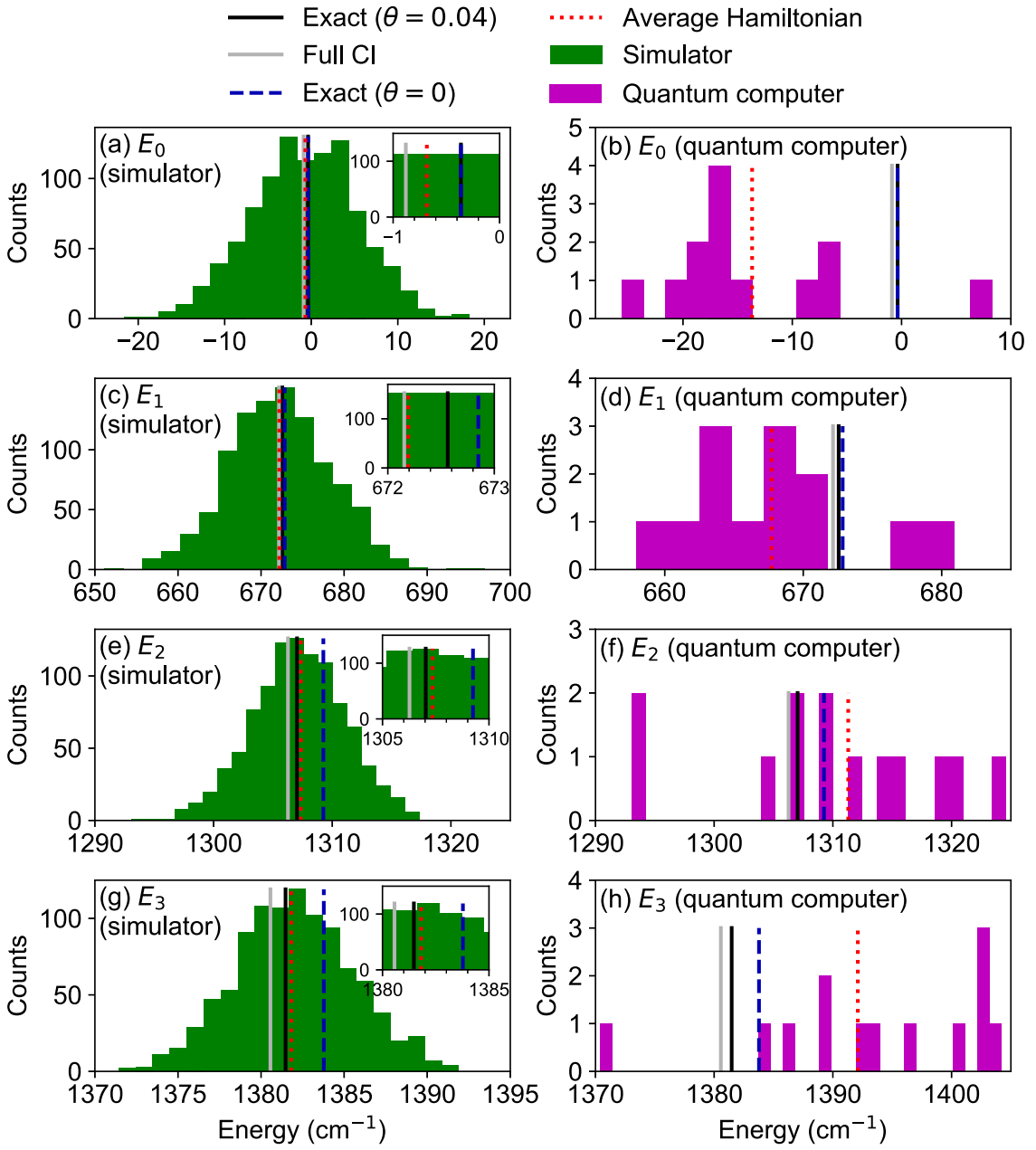

FIG. 3. Histograms of the energy eigenvalues $E_n^{(i)}$ for $n = 0$ (the ground state) and $n = 1, 2, 3$ (excited states). The green histograms shown in the left column in (a), (c), (e), and (g) are obtained by the *qasm_simulator* with the error model *FakeRome*, and the magenta bars shown in the right column in (b), (d), (f), and (h) are obtained by the *ibmq_rome* quantum computer at IBM Quantum. Also shown are the energy $\overline{E}_n$ obtained by diagonalizing the average Hamiltonian $\overline{\boldsymbol{h}}'$, the exact energies $E_n^{\text{exact}}(\theta)$ at $\theta = 0$ and 0.04, and the full CI energy E_n^{FCI}. The insets in the left column show expanded views around $\overline{E}_n$.

The experimental rovibrational transition frequencies of polyatomic molecules such as C_6H_6 [53], CH_3OH [54]. and CO_2 [55] obtained by high-resolution vibrational spectroscopy typically have uncertainties as small as 0.001 cm^{-1}. In order to reach the uncertainty achieved in high-resolution vibrational spectroscopy, we need to introduce improved error mitigation methods and lower the noise level in the quantum computer significantly.

The energy eigenvalues obtained using the *ibmq_rome* quantum computer at IBM Quantum, shown with magenta bars in in Figs. 3(b), 3(d), 3(f), and 3(h), do not agree well with the exact energies $E_n^{\text{exact}}(\theta = 0.04)$ because of the limited number of evaluations $M = 13$. We expect that the same uncertainty of below 1 cm^{-1} could be obtained also using *ibmq_rome* if the number of evaluations of the corrected Hamiltonian matrix $\boldsymbol{h}'$ is increased to the same value of $M = 1000$ as that used for the simulator.

We comment that, because of the limited number of basis functions ($v_{\max} = 2$), the inclusion of two modes out of three, and the truncation of the anharmonic potential to the third-order terms, the excitation energies calculated within the present model need to be regarded as rough estimates

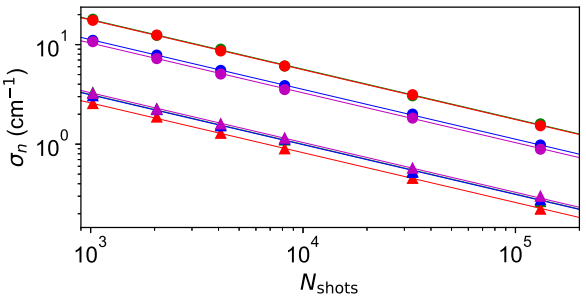

FIG. 4. Uncertainty σ_n of the energy eigenvalues E_0 (green symbols), E_1 (red symbols), E_2 (blue symbols), and E_3 (magenta symbols). The uncertainties obtained by the simulator including noise are shown with filled circles and the uncertainties obtained by a simulator without using a noise model are shown with triangles. The curve for E_1 almost completely overlaps that of E_0 in the case of the results obtained using the simulator with noise (filled circles) and the curve for E_2 almost completely overlaps that of E_0 in the case of the results obtained using the simulator without noise (filled triangles), The solid lines are fits to the expression $\sigma_n^{(\text{fit})} = A_n N_{\text{shots}}^{-1/2}$, where A_n are constants whose numerical values are given in Table II.

of the excitation energies. For the Fermi resonance pair, we obtain $\Delta E_2 = E_2 - E_0 = 1307$ cm^{-1} and $\Delta E_3 = E_3 - E_0 = 1381$ cm^{-1}, while the experimental excitation energies are $\Delta E_2^{\text{expt}} = 1285$ cm^{-1} and $\Delta E_3^{\text{expt}} = 1388$ cm^{-1} [28,29,32].

Finally, we investigate the dependence of the uncertainty σ_n, defined in Eq. (34), on the number of shots N_{shots}. We expect that σ_n should depend on N_{shots} approximately as $\sigma_n = A_n N_{\text{shots}}^{-1/2}$, where A_n is a constant, but the constant A_n depends on the details of the quantum computer and the depth of the circuits and has to be estimated from the simulation. In Fig. 4, we show the uncertainty σ_n for the energy histograms $E_n^{(i)}$ as a function of N_{shots}. We also show the result of a simulation using the *qasm_simulator* without including an error model, which means that the statistical uncertainty only arises from the finite number of N_{shots} and, in the limit $N_{\text{shots}} \to \infty$, we obtain the exact eigenenergies $E_n^{\text{exact}}(\theta = 0.04)$.

The data shown in Fig. 4 demonstrate that the presence of noise simulated by the noise model increases the statistical uncertainty σ_n by approximately a factor of 6 for E_0 and E_1 and a factor of 3 for E_2 and E_3. In order to estimate the required value N_{shots} to obtain a given value of σ_n, we have fitted the curves shown in Fig. 4 to the expression $\sigma_n^{(\text{fit})} = A_n N_{\text{shots}}^{-1/2}$, where A_n is a constant. The numerical values for A_n are shown in Table II.

Using the obtained values of A_n we can estimate the required value of N_{shots} for obtaining the uncertainty $\sigma_n = u$ in the presence of noise as $N_{\text{shots}}(\sigma_n = u) = (u/A_n)^2$. For $u = 0.2$ cm^{-1}, we obtain $N_{\text{shots}}(\sigma_{0,1} = 0.2\ \text{cm}^{-1}) \approx 8 \times 10^6$ for E_0 and E_1 and $N_{\text{shots}}(\sigma_{2,3} = 0.2\ \text{cm}^{-1}) \approx 3 \times 10^6$ for E_2 and E_3. These values are consistent with the statistical uncertainty of 0.2 cm^{-1} obtained for the average energies shown in the first row of Table I, because the average energies are obtained as an average of $M = 1000$ evaluations of the Hamiltonian matrix and each quantum circuit is executed $N_{\text{shots}} = 8192$ times, resulting in an effective number $MN_{\text{shots}} \approx 8 \times 10^6$ executions.

TABLE II. Numerical values of A_n for $n = 0, \ldots, 3$ in units of cm^{-1}. "Simulator (noise)" refers to results obtained using the *qasm_simulator* including a noise model and "Simulator (no noise)" refers to results obtained using the *qasm_simulator* without a noise model.

	Simulator (noise)	Simulator (no noise)
A_0	566.04	99.71
A_1	558.55	82.05
A_2	354.79	98.72
A_3	327.67	103.86

IV. SUMMARY

We have shown how vibrational energy levels of a model CO_2 molecule can be obtained on a quantum computer. By employing a modified version of the MC-VQE method, combining four different error mitigation methods, and evaluating the quantum circuits a total of $N_{\text{shots}} \times M \approx 8 \times 10^6$ times, we obtain the energy eigenvalues with an accuracy of better than 1 cm^{-1}. The most important error mitigation method is the correction of the constant shift of the Hamiltonian matrix caused by noise. Our results demonstrate that vibrational eigenvalues can be reliably evaluated on a quantum computer even for strong anharmonic resonances by which unperturbed vibrational levels are strongly mixed.

ACKNOWLEDGMENTS

The authors thank Dr. T. Nishi for his valuable comments. This work is partly supported by UTokyo Quantum Initiative. We acknowledge the use of IBM Quantum services for this work.

APPENDIX A: MAPPING OF THE HAMILTONIAN TO QUBIT FORM

In the compact mapping, which is also called the binary mapping, we use the binary representation of the vibrational quantum numbers v_1 and v_2 and map a harmonic-oscillator basis state to a qubit basis state according to

$$|v_2, v_1\rangle = |\text{bin}(v_2)\ \text{bin}(v_1)\rangle, \tag{A1}$$

where $\text{bin}(v) = p_1 p_0$ with p_i satisfying $\sum_{i=0}^{1} 2^i p_i = v$. For example, $|2, 1\rangle = |10\ 01\rangle$. The compact mapping requires a total of four qubits given that we employ $v_{\max} = 2$.

After having mapped the harmonic-oscillator basis functions to qubits, we can map the Hamiltonian to a sum of products of Pauli matrices according to the procedures described in Ref. [56]. By rewriting a single-qubit operator $|i\rangle\langle j|$ in terms of the Pauli matrices σ_x, σ_y, σ_z and the identity matrix I as

$$\begin{aligned} |0\rangle\langle 0| &= \tfrac{1}{2}(I + \sigma_z), \quad |0\rangle\langle 1| = \tfrac{1}{2}(\sigma_x + i\sigma_y), \\ |1\rangle\langle 0| &= \tfrac{1}{2}(\sigma_x - i\sigma_y) \quad |1\rangle\langle 1| = \tfrac{1}{2}(I - \sigma_z), \end{aligned} \tag{A2}$$

a general many-qubit operator can be mapped to sums of Pauli matrix products. For two qubits we have

$$|v_2', v_1'\rangle\langle v_2, v_1| = |q_3' q_2'\ q_1' q_0'\rangle\langle q_3 q_2\ q_1 q_0| = |q_3'\rangle\langle q_3| \otimes |q_2'\rangle\langle q_2| \otimes |q_1'\rangle\langle q_1| \otimes |q_0'\rangle\langle q_0|. \tag{A3}$$

The Hamiltonian matrix is expressed as

$$\boldsymbol{H} = \sum_{v_2', v_1', v_2, v_1=0}^{v_{\max}} H_{v_2' v_1' v_2 v_1} |v_2', v_1'\rangle\langle v_2, v_1| = \sum_{i=1}^{L} u_i P_i, \tag{A4}$$

where P_i is a product of Pauli matrices acting on the qubits (for example, $\sigma_z \otimes \sigma_z \otimes \sigma_y \otimes \sigma_y$) and u_i is a numerical coefficient. In Eq. (A4), $H_{v_2' v_1' v_2 v_1} = \langle v_2', v_1'|H|v_2, v_1\rangle$ are the matrix elements of the Hamiltonian (1). The numerical evaluation of $H_{v_2' v_1' v_2 v_1}$ is most conveniently done by first rewriting the Hamiltonian (1) in terms of creation and annihilation operators. We obtain a total number of $L = 40$ terms in the qubit Hamiltonian.

The qubit Hamiltonian matrix can be written as a sum of the uncoupled harmonic-oscillator Hamiltonian H_0 and the anharmonic coupling Hamiltonian H_I:

$$\boldsymbol{H} = \boldsymbol{H}_0 + \boldsymbol{H}_I = \sum_{i=1}^{L_0} u_{0i} P_{0i} + \sum_{i=1}^{L_I} u_{Ii} P_{Ii}. \tag{A5}$$

We obtain

$$\begin{aligned}\boldsymbol{H}_0/\mathrm{cm}^{-1} = {} & 1140.28IIII + 380.09III\sigma_z \\ & - 127.77II\sigma_z I + 127.77I\sigma_z II \\ & + 380.09I\sigma_z II - 887.96II\sigma_z\sigma_z \\ & - 42.59I\sigma_z\sigma_z I - 295.99I\sigma_z\sigma_z\sigma_z \\ & + 126.7I\sigma_z I\sigma_z + 42.59\sigma_z II\sigma_z \\ & - 126.7\sigma_z I\sigma_z I - 211.88\sigma_z I\sigma_z\sigma_z \\ & - 632.41\sigma_z\sigma_z II - 210.8\sigma_z\sigma_z I\sigma_z \\ & - 41.52\sigma_z\sigma_z\sigma_z I + 380.09\sigma_z\sigma_z\sigma_z\sigma_z\end{aligned} \tag{A6}$$

and

$$\begin{aligned}\boldsymbol{H}_I/\mathrm{cm}^{-1} = {} & 11.51III\sigma_x + 11.51II\sigma_z\sigma_x \\ & - 9.47II\sigma_x\sigma_x - 9.47II\sigma_y\sigma_y \\ & + 3.84I\sigma_z I\sigma_x - 9.37\sigma_z II\sigma_x \\ & + 9.34\sigma_x II\sigma_x + 9.34\sigma_x I\sigma_z\sigma_x \\ & + 3.84I\sigma_z\sigma_z\sigma_x - 9.37\sigma_z I\sigma_z\sigma_x \\ & + 9.34\sigma_x\sigma_z I\sigma_x + 9.34\sigma_x\sigma_z\sigma_z\sigma_x \\ & - 3.16I\sigma_z\sigma_x\sigma_x - 3.16I\sigma_z\sigma_y\sigma_y \\ & - 21.84\sigma_z I\sigma_x\sigma_x - 21.84\sigma_z I\sigma_y\sigma_y \\ & + 13.21\sigma_x I\sigma_x\sigma_x + 13.21\sigma_x I\sigma_y\sigma_y \\ & - 17.05\sigma_z\sigma_z I\sigma_x - 17.05\sigma_z\sigma_z\sigma_z\sigma_x \\ & - 15.52\sigma_z\sigma_z\sigma_x\sigma_x - 15.52\sigma_z\sigma_z\sigma_y\sigma_y \\ & + 13.21\sigma_x\sigma_z\sigma_x\sigma_x + 13.21\sigma_x\sigma_z\sigma_y\sigma_y,\end{aligned} \tag{A7}$$

$$\frac{1}{\sqrt{2}}(|00\ 01\rangle + |01\ 00\rangle) =$$

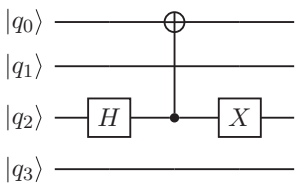

FIG. 5. Circuit for the creation of the superposition state $(|00\ 01\rangle + |01\ 00\rangle)/\sqrt{2}$. The circuit diagram is drawn using the QUANTIKZ package [57].

where we have omitted the direct product symbols $\otimes$ for brevity. The rightmost Pauli matrix acts on qubit 0, the second operator to the right acts on qubit 1, and so on.

APPENDIX B: EVALUATION OF MATRIX ELEMENTS

As described in Ref. [20], a matrix element $\langle\chi_m|H|\chi_n\rangle$ can be obtained by evaluating the expectation values of H in the states

$$|\chi_{mn}^{\pm}\rangle = U(\boldsymbol{\theta})|\phi_{mn}^{\pm}\rangle, \tag{B1}$$

where

$$|\phi_{mn}^{\pm}\rangle = \frac{1}{\sqrt{2}}(|\phi_m\rangle \pm |\phi_n\rangle). \tag{B2}$$

We have

$$\langle\chi_m|H|\chi_n\rangle = \tfrac{1}{2}(\langle\chi_{mn}^{+}|H|\chi_{mn}^{+}\rangle - \langle\chi_{mn}^{-}|H|\chi_{mn}^{-}\rangle). \tag{B3}$$

Quantum circuits representing the $|\phi_{mn}^{\pm}\rangle$ states can be constructed by combining a Hadamard gate and a CNOT gate. An example of the creation of the state $(|0, 1\rangle + |1, 0\rangle)/\sqrt{2} = (|00\ 01\rangle + |01\ 00\rangle)/\sqrt{2}$ is displayed in Fig. 5.

APPENDIX C: SCALING

In this Appendix, we present estimates for the scaling of the number of terms in the qubit Hamiltonian and the number of gates required in the MC-VQE method for a large molecule with many vibrational modes. In the discussion below, K denotes the number of qubits, N denotes the number of atoms in a molecule, V $(= 3N - 6)$ denotes the number of vibrational modes, and κ denotes the number of basis functions by which each vibrational mode is expanded, that is, the same number of basis functions κ is employed for each vibrational mode. In deriving the V and κ dependence of the scaling relations below, we treat both the highest order p of the anharmonic coupling term in the Hamiltonian and the excitation order c of the unitary coupled-cluster operator as constants, which means that we do not consider the form of the p- and c-dependent prefactors.

In the compact mapping, the number of qubits K required to describe a vibrational wave function having κ^V amplitudes is given by

$$K = V\ \log_2 \kappa, \tag{C1}$$

because each mode can be represented by $\log_2 \kappa$ qubits.

The Hamiltonian (1) having third-order terms in the anharmonic potential contains $O(V^3)$ terms. A Hamiltonian

having anharmonic coupling terms up to order p contains $O(V^p)$ terms and each term in the Hamiltonian can be mapped to $O(\kappa^{2p})$ number of sigma-matrix strings [56], so that a total number of terms in the qubit Hamiltonian becomes

$$N_{\rm qH} = O(V^p \kappa^{2p}). \tag{C2}$$

The single-excitation coupled-cluster operator $T(\boldsymbol{\theta}) - T^\dagger(\boldsymbol{\theta})$ defined in Eq. (11) is composed of $O(V\kappa^2)$ terms of the form $|v'\rangle\langle v|_\ell$, where v and v' denote respectively the vibrational quantum numbers before and after the excitation and ℓ labels the vibrational mode. Each term can be mapped to $O(\kappa)$ sigma-matrix strings, each of which contains $\log_2 \kappa$ sigma matrices. For a unitary coupled-cluster operator exciting c modes, we get $O(V^c\kappa^{2c})$ terms composed of $O(\kappa^c)$ sigma-matrix strings, each of which contains $c \log_2 \kappa$ sigma matrices. One measure of the complexity of a quantum circuit is the number of CNOT gates included in the circuit. In the case of the unitary operator $U(\boldsymbol{\theta}) = e^{T(\boldsymbol{\theta})-T^\dagger(\boldsymbol{\theta})}$, we need to implement the exponentiation of sigma-matrix strings of length $c \log_2 \kappa$, which requires $O(\log_2 \kappa)$ CNOT gates [56]. Therefore, the total number of CNOT gates required for the implementation of $U(\boldsymbol{\theta})$ becomes

$$N_{U(\boldsymbol{\theta})\rm CNOT} = O(V^c \kappa^{3c} \log_2 \kappa). \tag{C3}$$

The number of CNOT gates required for the implementation of the $|\phi^\pm_{mn}\rangle$ states defined in Eq. (B2) is $N_{|\phi^\pm_{mn}\rangle\rm CNOT} = O(K) = O(V \log_2 \kappa)$ because we can create a two-state superposition state of two arbitrary qubit states using $O(K)$ CNOT gates. For large κ, $N_{U(\boldsymbol{\theta})\rm CNOT} \gg N_{|\phi^\pm_{mn}\rangle\rm CNOT}$. The total number of CNOT gates required for the preparation of the circuit representing the trial state $|\chi^\pm_{mn}(\boldsymbol{\theta})\rangle = U(\boldsymbol{\theta})|\phi^\pm_{mn}\rangle$ is therefore

$$N_{\rm CNOT} = N_{U(\boldsymbol{\theta})\rm CNOT} = O(V^c \kappa^{3c} \log_2 \kappa). \tag{C4}$$

Each circuit has to be measured $N_{\rm qH}$ times to evaluate one matrix element. Note that both $N_{\rm CNOT}$ and $N_{\rm qH}$ scale polynomially with respect to the number of modes V.

In the MC-VQE method, we evaluate all matrix elements $\langle\phi_m|U^\dagger(\boldsymbol{\theta})HU(\boldsymbol{\theta})|\phi_n\rangle$ between single-mode excited basis functions $|\phi_m\rangle$. This means that we have to evaluate

$$N_{\rm matrix} = O(V^2\kappa^2) \tag{C5}$$

number of matrix elements to obtain the eigenenergies. Therefore, in order to obtain the eigenvalues in the MC-VQE method, we have to evaluate

$$N_{\rm circ} = N_{\rm matrix} N_{\rm qH} = O(V^{p+2}\kappa^{2p+2}) \tag{C6}$$

circuits, each of which contains $N_{\rm CNOT}$ CNOT gates.

[1] B. Bauer, S. Bravyi, M. Motta, and G. K.-L. Chan, Quantum algorithms for quantum chemistry and quantum materials science, Chem. Rev. **120**, 12685 (2020).

[2] S. McArdle, S. Endo, A. Aspuru-Guzik, S. C. Benjamin, and X. Yuan, Quantum computational chemistry, Rev. Mod. Phys. **92**, 015003 (2020).

[3] F. Arute, K. Arya, R. Babbush, D. Bacon, J. C. Bardin, R. Barends, R. Biswas, S. Boixo, F. G. S. L. Brandao, D. A. Buell, B. Burkett, Y. Chen, Z. Chen, B. Chiaro, R. Collins, W. Courtney, A. Dunsworth, E. Farhi, B. Foxen, A. Fowler *et al.*, Quantum supremacy using a programmable superconducting processor, Nature (London) **574**, 505 (2019).

[4] H.-S. Zhong, H. Wang, Y.-H. Deng, M.-C. Chen, L.-C. Peng, Y.-H. Luo, J. Qin, D. Wu, X. Ding, Y. Hu, P. Hu, X.-Y. Yang, W.-J. Zhang, H. Li, Y. Li, X. Jiang, L. Gan, G. Yang, L. You, Z. Wang *et al.*, Quantum computational advantage using photons, Science **370**, 1460 (2020).

[5] Google AI Quantum and Collaborators, Hartree-Fock on a superconducting qubit quantum computer, Science **369**, 1084 (2020).

[6] B. P. Lanyon, J. D. Whitfield, G. G. Gillett, M. E. Goggin, M. P. Almeida, I. Kassal, J. D. Biamonte, M. Mohseni, B. J. Powell, M. Barbieri, A. Aspuru-Guzik, and A. G. White, Towards quantum chemistry on a quantum computer, Nat. Chem. **2**, 106 (2010).

[7] P. J. J. O'Malley, R. Babbush, I. D. Kivlichan, J. Romero, J. R. McClean, R. Barends, J. Kelly, P. Roushan, A. Tranter, N. Ding, B. Campbell, Y. Chen, Z. Chen, B. Chiaro, A. Dunsworth, A. G. Fowler, E. Jeffrey, E. Lucero, A. Megrant, J. Y. Mutus *et al.*, Scalable Quantum Simulation of Molecular Energies, Phys. Rev. X **6**, 031007 (2016).

[8] A. Kandala, A. Mezzacapo, K. Temme, M. Takita, M. Brink, J. M. Chow, and J. M. Gambetta, Hardware-efficient variational quantum eigensolver for small molecules and quantum magnets, Nature (London) **549**, 242 (2017).

[9] J. I. Colless, V. V. Ramasesh, D. Dahlen, M. S. Blok, M. E. Kimchi-Schwartz, J. R. McClean, J. Carter, W. A. de Jong, and I. Siddiqi, Computation of Molecular Spectra on a Quantum Processor with an Error-Resilient Algorithm, Phys. Rev. X **8**, 011021 (2018).

[10] C. Hempel, C. Maier, J. Romero, J. McClean, T. Monz, H. Shen, P. Jurcevic, B. P. Lanyon, P. Love, R. Babbush, A. Aspuru-Guzik, R. Blatt, and C. F. Roos, Quantum Chemistry Calculations on a Trapped-Ion Quantum Simulator, Phys. Rev. X **8**, 031022 (2018).

[11] Y. Wang, F. Dolde, J. Biamonte, R. Babbush, V. Bergholm, S. Yang, I. Jakobi, P. Neumann, A. Aspuru-Guzik, J. D. Whitfield, and J. Wrachtrup, Quantum simulation of helium hydride cation in a solid-state spin register, ACS Nano **9**, 7769 (2015).

[12] A. G. Császár, C. Fábri, T. Szidarovszky, E. Mátyus, T. Furtenbacher, and G. Czakó, The fourth age of quantum chemistry: Molecules in motion, Phys. Chem. Chem. Phys. **14**, 1085 (2012).

[13] A. G. Császár, I. Simkó, T. Szidarovszky, G. C. Groenenboom, T. Karman, and A. van der Avoird, Rotational-vibrational resonance states, Phys. Chem. Chem. Phys. **22**, 15081 (2020).

[14] S. McArdle, A. Mayorov, X. Shan, S. Benjamin, and X. Yuan, Digital quantum simulation of molecular vibrations, Chem. Sci. **10**, 5725 (2019).

[15] N. P. D. Sawaya and J. Huh, Quantum algorithm for calculating molecular vibronic spectra, J. Phys. Chem. Lett. **10**, 3586 (2019).

[16] P. J. Ollitrault, A. Baiardi, M. Reiher, and I. Tavernelli, Hardware efficient quantum algorithms for vibrational structure calculations, Chem. Sci. **11**, 6842 (2020).

[17] J. Huh, G. G. Guerreschi, B. Peropadre, J. R. McClean, and A. Aspuru-Guzik, Boson sampling for molecular vibronic spectra, Nat. Photon. **9**, 615 (2015).

[18] S. Jahangiri, J. M. Arrazola, N. Quesada, and A. Delgado, Quantum algorithm for simulating molecular vibrational excitations, Phys. Chem. Chem. Phys. **22**, 25528 (2020).

[19] C. S. Wang, J. C. Curtis, B. J. Lester, Y. Zhang, Y. Y. Gao, J. Freeze, V. S. Batista, P. H. Vaccaro, I. L. Chuang, L. Frunzio, L. Jiang, S. M. Girvin, and R. J. Schoelkopf, Efficient Multiphoton Sampling of Molecular Vibronic Spectra on a Superconducting Bosonic Processor, Phys. Rev. X **10**, 021060 (2020).

[20] R. M. Parrish, E. G. Hohenstein, P. L. McMahon, and T. J. Martínez, Quantum Computation of Electronic Transitions Using a Variational Quantum Eigensolver, Phys. Rev. Lett. **122**, 230401 (2019).

[21] D. S. Abrams and S. Lloyd, Quantum Algorithm Providing Exponential Speed Increase for Finding Eigenvalues and Eigenvectors, Phys. Rev. Lett. **83**, 5162 (1999).

[22] R. Babbush, C. Gidney, D. W. Berry, N. Wiebe, J. McClean, A. Paler, A. Fowler, and H. Neven, Encoding Electronic Spectra in Quantum Circuits with Linear T Complexity, Phys. Rev. X **8**, 041015 (2018).

[23] L.-A. Wu, M. S. Byrd, and D. A. Lidar, Polynomial-Time Simulation of Pairing Models on a Quantum Computer, Phys. Rev. Lett. **89**, 057904 (2002).

[24] T. Albash and D. A. Lidar, Adiabatic quantum computation, Rev. Mod. Phys. **90**, 015002 (2018).

[25] Y. Sun, J.-Y. Zhang, M. S. Byrd, and L.-A. Wu, Trotterized adiabatic quantum simulation and its application to a simple all-optical system, New J. Phys. **22**, 053012 (2020).

[26] H. Abraham *et al.*, Qiskit: An open-source framework for quantum computing, https://qiskit.org

[27] IBM Quantum team, https://quantum-computing.ibm.com, *ibmq_rome* v1.3.9.

[28] E. Fermi, Über den Ramaneffekt des Kohlendioxyds, Z. Phys. **71**, 250 (1931).

[29] V. Rodriguez-Garcia, S. Hirata, K. Yagi, K. Hirao, T. Taketsugu, I. Schweigert, and M. Tasumi, Fermi resonance in CO_2: A combined electronic coupled-cluster and vibrational configuration-interaction prediction, J. Chem. Phys. **126**, 124303 (2007).

[30] K. Yamanouchi, N. Ikeda, S. Tsuchiya, D. M. Jonas, J. K. Lundberg, G. W. Adamson, and R. W. Field, Vibrationally highly excited acetylene as studied by dispersed fluorescence and stimulated emission pumping spectroscopy: Vibrational assignment of the feature states, J. Chem. Phys. **95**, 6330 (1991).

[31] T. Baer and W. L. Hase, *Unimolecular Reaction Dynamics – Theory and Experiments* (Oxford University Press, New York, 1996).

[32] I. Suzuki, General anharmonic force constants of carbon dioxide, J. Mol. Spectrosc. **25**, 479 (1968).

[33] L. Veis, J. Višňák, H. Nishizawa, H. Nakai, and J. Pittner, Quantum chemistry beyond Born-Oppenheimer approximation on a quantum computer: A simulated phase estimation study, Int. J. Quantum Chem. **116**, 1328 (2016).

[34] A. Peruzzo, J. McClean, P. Shadbolt, M.-H. Yung, X.-Q. Zhou, P. J. Love, A. Aspuru-Guzik, and J. L. O'Brien, A variational eigenvalue solver on a photonic quantum processor, Nat. Commun. **5**, 4213 (2014).

[35] J. R. McClean, M. E. Kimchi-Schwartz, J. Carter, and W. A. de Jong, Hybrid quantum-classical hierarchy for mitigation of decoherence and determination of excited states, Phys. Rev. A **95**, 042308 (2017).

[36] Y. Li, J. Hu, X.-M. Zhang, Z. Song, and M.-H. Yung, Variational quantum simulation for quantum chemistry, Adv. Theor. Simul. **2**, 1800182 (2019).

[37] S. Endo, Z. Cai, S. C. Benjamin, and X. Yuan, Hybrid quantum-classical algorithms and quantum error mitigation, J. Phys. Soc. Jpn. **90**, 032001 (2021).

[38] A. G. Taube and R. J. Bartlett, New perspectives on unitary coupled-cluster theory, Int. J. Quantum Chem. **106**, 3393 (2006).

[39] F. A. Evangelista, G. K.-L. Chan, and G. E. Scuseria, Exact parameterization of fermionic wave functions via unitary coupled cluster theory, J. Chem. Phys. **151**, 244112 (2019).

[40] J. Lee, W. J. Huggins, M. Head-Gordon, and K. B. Whaley, Generalized unitary coupled cluster wave functions for quantum computation, J. Chem. Theory Comput. **15**, 311 (2019).

[41] J. Romero, R. Babbush, J. R. McClean, C. Hempel, P. J. Love, and A. Aspuru-Guzik, Strategies for quantum computing molecular energies using the unitary coupled cluster ansatz, Quantum Sci. Technol. **4**, 014008 (2019).

[42] W. Mizukami, K. Mitarai, Y. O. Nakagawa, T. Yamamoto, T. Yan, and Y.-y. Ohnishi, Orbital optimized unitary coupled cluster theory for quantum computer, Phys. Rev. Research **2**, 033421 (2020).

[43] B. Cooper and P. J. Knowles, Benchmark studies of variational, unitary and extended coupled cluster methods, J. Chem. Phys. **133**, 234102 (2010).

[44] M. A. Nielsen and I. L. Chuang, *Quantum Computation and Quantum Information* (Cambridge University Press, Cambridge, UK, 2010).

[45] See the Supplemental Material in S. E. Smart and D. A. Mazziotti, Lowering tomography costs in quantum simulation with a symmetry projected operator basis, Phys. Rev. A **103**, 012420 (2021).

[46] Y. Li and S. C. Benjamin, Efficient Variational Quantum Simulator Incorporating Active Error Minimization, Phys. Rev. X **7**, 021050 (2017).

[47] K. Temme, S. Bravyi, and J. M. Gambetta, Error Mitigation for Short-Depth Quantum Circuits, Phys. Rev. Lett. **119**, 180509 (2017).

[48] S. Endo, S. C. Benjamin, and Y. Li, Practical Quantum Error Mitigation for Near-Future Applications, Phys. Rev. X **8**, 031027 (2018).

[49] A. Kandala, K. Temme, A. D. Córcoles, A. Mezzacapo, J. M. Chow, and J. M. Gambetta, Error mitigation extends the computational reach of a noisy quantum processor, Nature (London) **567**, 491 (2019).

[50] D. Wecker, M. B. Hastings, and M. Troyer, Progress towards practical quantum variational algorithms, Phys. Rev. A **92**, 042303 (2015).

[51] M. Schuld, V. Bergholm, C. Gogolin, J. Izaac, and N. Killoran, Evaluating analytic gradients on quantum hardware, Phys. Rev. A **99**, 032331 (2019).

[52] A. Mari, T. R. Bromley, and N. Killoran, Estimating the gradient and higher-order derivatives on quantum hardware, Phys. Rev. A **103**, 012405 (2021).

[53] M. Snels, H. Hollenstein, and M. Quack, High resolution FTIR spectra and analysis of the ν_{11} fundamental band of $^{13}C_6H_6$, Chem. Phys. Lett. **350**, 57 (2001).

[54] L.-H. Xu, R. M. Lees, P. Wang, L. R. Brown, I. Kleiner, and J. W. C. Johns, New assignments, line intensities, and HITRAN database for CH_3OH at 10 μm, J. Mol. Spectrosc. **228**, 453 (2004).

[55] S. Tashkun, V. Perevalov, R. Gamache, and J. Lamouroux, CDSD-296, high resolution carbon dioxide spectroscopic databank: Version for atmospheric applications, J. Quant. Spectrosc. Radiat. Transfer **152**, 45 (2015).

[56] N. P. D. Sawaya, T. Menke, T. H. Kyaw, S. Johri, A. Aspuru-Guzik, and G. G. Guerreschi, Resource-efficient digital quantum simulation of d-level systems for photonic, vibrational, and spin-s Hamiltonians, npj Quantum Inf. **6**, 49 (2020).

[57] A. Kay, Tutorial on the quantikz package, arXiv:1809.03842 [quant-ph].